

PAPER

Hybrid Analysis of Human Exposure from Base-Station Antennas in Underground Environment

Jianqing WANG^{†a)}, *Member*, Masayuki KOMATSU[†], *Student Member*, Osamu FUJIWARA[†],
and Shinji UEBAYASHI^{††}, *Members*

SUMMARY In this study we have employed an effective technique for dosimetric analyses of base station antennas in an underground environment. The technique combines a ray-tracing method and the finite-difference time-domain (FDTD) method to calculate the specific absorption rate (SAR) in the human body. The ray-tracing method was applied to evaluate the incident fields in relation to the exposed subject in a three-dimensional space, while the FDTD method was used to calculate the detailed SAR distributions in the human body. A scenario under an underground passage with the installation of a top-loaded monopole antenna was analyzed to investigate the relationship between the actual antenna exposure and a plane-wave exposure. The results show that the plane-wave exposure overestimated the whole-body average SAR in most cases, although this was not always true for peak SAR. The finding implies not only the usefulness of the present uniform-exposure-based reference level for the whole-body average SAR evaluation but also the necessity of modeling actual underground environment for high-precision local peak SAR evaluation.

key words: underground environment, base station antenna, SAR, ray-tracing method, FDTD method, safety evaluation

1. Introduction

With the rapid spread of mobile communications, the installation of base station antennas in underground environments is increasing. In the compliance assessment of these base station antennas, an incident electric field or power density is being used as a reference level, which should never yield a larger whole-body average specific absorption rate (SAR) than the basic limit, e.g. 0.4 W/kg for occupational exposure or 0.08 W/kg for public exposure [1], [2]. The relationship between the reference level and the whole-body average SAR, however, was derived based on a free-space plane-wave exposure. The base station exposure in an underground environment is actually different from a plane-wave exposure because of the existence of walls, floor, ceiling and so on. For such a non-uniform exposure, the electric field averaged over a human-occupied volume is required and must be compared with the reference level. This raises the question as to whether the present reference level may still be applicable to such a complicated environment, and therefore the need arises for dosimetry evaluation of human exposure in the real environment.

In this study, we investigated a scenario in an underground passage to examine the relationship between the actual SAR level and that derived from the free-space plane-wave exposure. The finite-difference time-domain method [3] is the most frequently used tool in SAR calculation at present. However, modeling an underground passage in the radio-frequency range requires huge memories and computation time because the entire computation region has to be divided into cells with dimensions smaller than $1/8$ – $1/10$ wavelength.

To cope with this problem, we employed a hybrid technique which combines a ray-tracing method and the scattered-field FDTD method for the SAR calculation in the human body. The basic idea was to use the ray-tracing method to calculate the incident field to the exposed human body in the whole underground passage, and then use the scattered-field FDTD method to calculate the detailed SAR distributions inside the human body. This should be of practical use in terms of calculation resources because the FDTD calculation was applied only to a small portion of the entire underground passage. This approach is similar to [4] but the data transfer is different between the ray-tracing method and the FDTD method. In [4], according to the equivalence principle, the incident fields obtained with the ray-tracing method were expressed in terms of the equivalent surface electric and magnetic currents, and were then used as excitations at a closed surface surrounding the human body. The FDTD algorithm operated on the total field (the incident field plus the scattered field) inside the closed surface, and operated only on the scattered field outside the closed surface. A connection was therefore necessary for the field components at the closed surface. Against this approach, we employ the scattered-field FDTD method in which the incident field in the entire region of analysis is directly used as the excitation. It avoids the employment of a connection algorithm at a surface surrounding the human body. The details will be described in 2.2.

In this paper, the modeling of the hybrid technique is first verified in comparison with the full-FDTD results. Then the relationship between the SAR in the underground passage and the SAR derived from plane-wave exposure is investigated.

Manuscript received January 30, 2006.

Manuscript revised May 29, 2006.

[†]The authors are with the Graduate School of Engineering, Nagoya Institute of Technology, Nagoya-shi, 466-8555 Japan.

^{††}The author is with the NTT DoCoMo Inc., Yokosuka-shi, 239-8536 Japan.

a) E-mail: wang@nitech.ac.jp

DOI: 10.1093/ietcom/e89-b.12.3411

2. Hybrid Technique for SAR Calculation

2.1 Ray-Tracing Method

The ray-tracing method [5], [6] provides a high-frequency and quick approximation of exact electric fields in a complex environment. The propagation of each ray from a source point is traced throughout the environment. The electric field at the receiving point is predicted by the sum of all of the rays reaching the point. As a first step in this study, according to the radiation pattern of a base station antenna, we took into account the transmission and reflection from the floor, ceiling and walls of the underground passage. The imaging theory was therefore applied, and the reflections upto five times were considered because more reflections hardly altered the field levels based on our simulation results for concrete. According to the geometric optic theory, the electric field at the receiving point from the m -th source (either original or imaging) point can be expressed as

$$E_m = \frac{\sqrt{K \cdot P_T \cdot G_T(m) \cdot G_R(m)} e^{-jkS_m}}{S_m} \cdot \prod \Gamma_{m,n} \quad (1)$$

where $K = \eta_0/4\pi$ (η_0 : the instant free-space impedance), k is the wave number, P_T is the transmitting power, S_m is the distance from the transmitting point to the receiving point, $G_T(m)$ and $G_R(m)$ are the transmitting and receiving gains, respectively, and $G_T(m)$ was obtained from the FDTD-calculated antenna radiation pattern. $\Gamma_{m,n}$ is the reflection coefficient of the m -th ray at the n -th plane in the Fresnel region, which is given as

$$\Gamma_{m,n}^{TM} = \frac{-\epsilon_c \cos \theta_{m,n} + \sqrt{\epsilon_c - \sin^2 \theta_{m,n}}}{\epsilon_c \cos \theta_{m,n} + \sqrt{\epsilon_c - \sin^2 \theta_{m,n}}} \quad (2)$$

$$\Gamma_{m,n}^{TE} = \frac{\cos \theta_{m,n} - \sqrt{\epsilon_c - \sin^2 \theta_{m,n}}}{\cos \theta_{m,n} + \sqrt{\epsilon_c - \sin^2 \theta_{m,n}}} \quad (3)$$

for TE and TM incidence, respectively, where ϵ_c is the complex permittivity of the reflection planes. In the above equations, the walls, floor and ceiling were characterized by ϵ_c ($\epsilon_c = \epsilon_r - j\sigma/\omega\epsilon_0$, ϵ_r : relative permittivity; σ : conductivity).

2.2 Scattered-Field FDTD Method

After obtaining the incident electric field E_i from the ray-tracing method in the human-occupied volume, at the second step, the scattered-field FDTD method [3] was used for the SAR calculation.

The total electric field E and magnetic field H in the presence of the human body can be expressed as

$$E = E_i + E_s, \quad H = H_i + H_s \quad (4)$$

where E_s and H_s are the scattered electric and magnetic fields, respectively. Substituting Eq. (4) into Maxwell equation, we have

$$\frac{\partial E_s}{\partial t} = -\frac{\sigma}{\epsilon} E_s + \frac{1}{\epsilon} \nabla \times H_s - \frac{\sigma}{\epsilon} E_i - \frac{\epsilon - \epsilon_0}{\epsilon} \frac{\partial E_i}{\partial t} \quad (5)$$

$$\frac{\partial H_s}{\partial t} = \frac{1}{\mu} \nabla \times E_s - \frac{\mu - \mu_0}{\mu} \frac{\partial H_i}{\partial t} \quad (6)$$

where ϵ is the permittivity and σ is the conductivity. The incident magnetic field H_i in Eq. (6) did not need to be considered because the human tissue is non-magnetic material, i.e., $\mu = \mu_0$. By discretizing the two equations both in the time and space domains, the scattered electric field E_s was obtained by using the FDTD scheme, and then the total electric field and the SAR inside the human body were calculated from Eq. (4) and $SAR = \sigma/\rho|E|^2$, respectively. It is clear that in this approach one does not need to assume a virtual closed surface to make use of the equivalence principle and therefore avoids the connection of field components inside and outside the closed surface.

It should be emphasized that the incident field is obtained with ray-tracing method in the absence of the human body. The existence of the human body induces a scattered field. The scattered field from the human body may reach the walls, ceiling and floor, and reflects again into the human body. This factor is not considered in the hybrid method. So the application of the method should be limited to the case where the above-mentioned reflection is insignificant. For the case of a human body in an underground passage, as long as the human body is not very close to the walls, the method should be applicable.

3. Results and Discussion

Figure 1 shows the geometry of a scenario under an underground passage. The walls, floor and ceiling were assumed to be concrete ($\epsilon_r = 6.76$, $\sigma = 0.0023$ S/m at 2 GHz [6]) with infinite thickness. Two monopole-type antennas were considered at 2 GHz. Either of them was mounted on the ceiling at the center of two sides of the walls. One antenna was a conventional 1/4-wavelength monopole with a ground

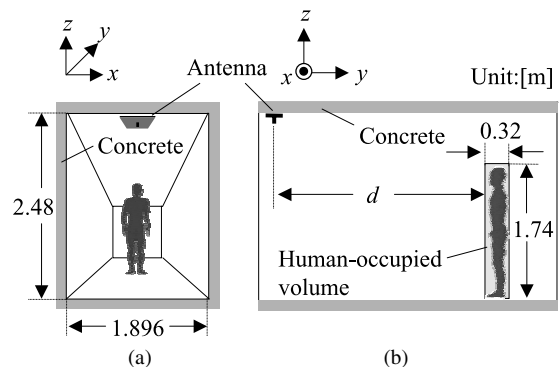


Fig. 1 Underground passage model. (a) front view and (b) side view.

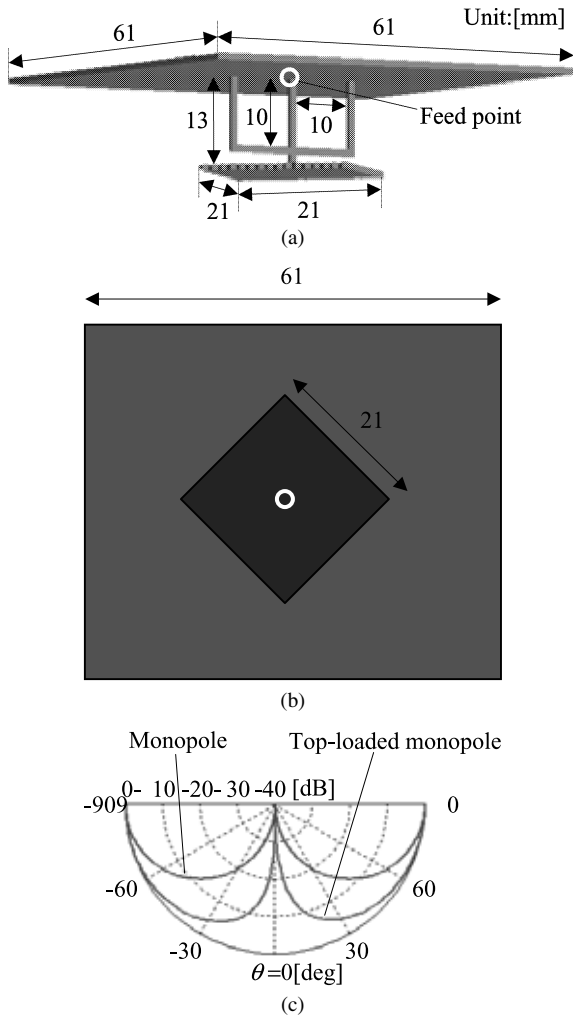


Fig. 2 Top-loaded monopole antenna. (a) 3-dimensional structure, (b) bottom view and (c) radiation pattern of the top-loaded monopole antenna.

plate of $0.32 \text{ m} \times 0.32 \text{ m}$, and the other antenna was a top-loaded monopole [7] that is being used in the actual underground environment. Figures 2(a) and (b) show the structure of the top-loaded monopole antenna, and Fig. 2(c) shows its FDTD-calculated radiation pattern together with the radiation pattern of the conventional monopole antenna. The top-loaded monopole antenna exhibits better directivity.

3.1 Propagation Characteristics

To examine the characteristics of the incident field in the absence of the human body, we first calculated the Poynting vector $S = E \times H$ at a distance of $d = 4.2 \text{ m}$ (28 free-space wavelengths at 2 GHz) from the antenna along the passage as shown in Fig. 1(b). Figure 3 shows the Poynting vector distribution at a vertical plane along the center line ($x = 0.0 \text{ m}$) of the passage from 4.2 to 4.7 m for the monopole antenna. It was clearly demonstrated that the incident field is not a plane-wave incidence in the underground environment, although the observed region is a far-field one. For a plane-wave incidence, the Poynting vectors should have the same

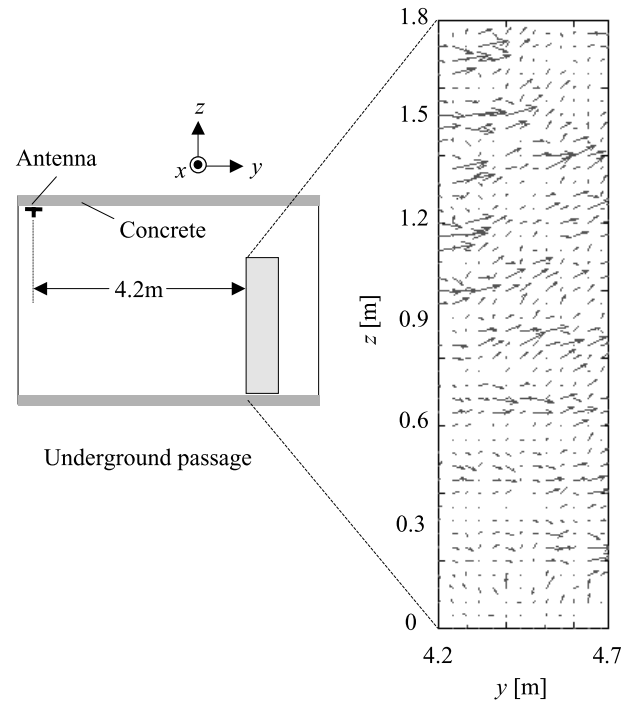


Fig. 3 Poynting vector distribution ($x = 0.0 \text{ m}$). The length denotes the magnitude, and the arrow denotes the direction of Poynting vectors.

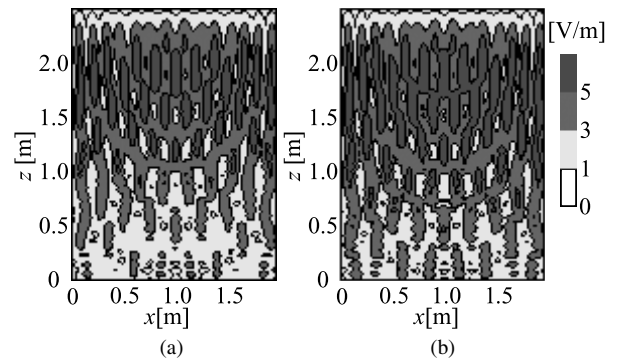


Fig. 4 Electric field distributions in the z - x plane ($d = 1.2 \text{ m}$). (a) monopole antenna and (b) top-loaded monopole antenna.

magnitude along the same direction.

Figure 4 shows the electric field distributions for the monopole and the top-loaded monopole antennas at a vertical plane (z - x plane) with a distance of $d = 1.2 \text{ m}$ from the antennas by using the ray-tracing method. In both of the two situations, the incident electric fields exhibited a very non-uniform distribution, i.e., stronger field levels in the top region and weaker field levels in the bottom region. The electric fields in the human-occupied volume are listed in Table 1, which show a variation up to four times between the minimum value and maximum value of the electric field induced by the monopole or top-loaded monopole antenna.

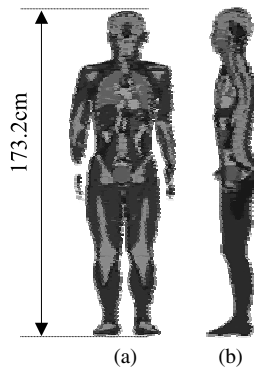
3.2 SAR Validation

Based on the hybrid technique, after obtaining the incident

Table 1 Comparison of electric fields in the human-occupied volume. ($d = 1.2$ m)

	Average E	Max E	Min E
Monopole	6.14	12.44	3.70
Top-loaded	6.14	11.82	2.82
Plane wave	6.14	6.14	6.14

Unit:[V/m]

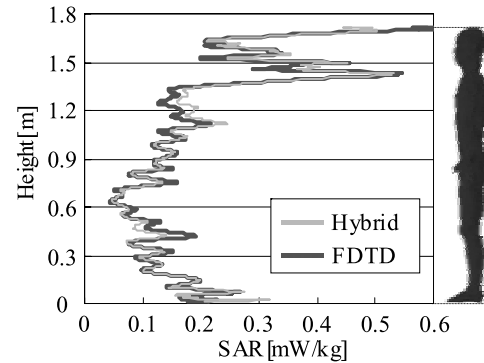
**Fig. 5** Human model. (a) front view and (b) side view.

electric field in the human-occupied volume using the ray-tracing method, we then calculated the SAR in the human body using the scattered-field FDTD method. The human-occupied volume was assumed at a distance of 1.2 m from the antenna. The human body model was developed based on anatomical data of a Japanese adult male [8]. The model has a height of 173 cm, a weight of 65 kg, and consists of 51 types of tissue in a resolution of 2 mm (Fig. 5). The dielectric properties of each tissue at 2 GHz were determined from the 4-cole-cole approximation based on Gabriel's data [9].

To verify the validity of the hybrid technique for the SAR calculation, we also performed a full-FDTD run for the monopole antenna. That is to say, the entire underground passage and the human body were modeled with the conventional FDTD method, in which the perfectly matched layers in the concrete were applied because we assumed infinitely thick concrete walls, floor and ceiling. Figure 6 compares the average SAR distributions along the height of the human body. The SAR derived from the hybrid technique agreed well with the full-FDTD result. The difference in the whole-body average SARs was within 5%, which ensures the validity of the hybrid technique for the SAR calculation.

3.3 Comparison with Plane-Wave Exposure

To investigate the relationship between the base station exposure in the underground passage and the free-space plane-wave exposure, we compared the SARs when they have the same incident electric field intensity. The plane wave was assumed to have a vertical polarization, i.e., z-directed in Fig. 1, because the top-loaded monopole antenna had a similar directivity to a vertical monopole antenna whose electric field is z-directed in the far-field region. Figure 7 shows the surface SAR distributions for the top-loaded monopole an-

**Fig. 6** Profile of layer-averaged SAR in whole-body.

tenna at a distance of 1.2 m from the antenna. The incident electric field intensity, as averaged over the human-occupied volume, was normalized to 6.14 V/m, i.e., 1/10 of the reference level of electric field for public exposure being specified in various safety guidelines. The actual level of base station antennas are considered to be similar to, or smaller than, this value. Also shown in the figure is the plane-wave exposure with the same incident electric field intensity as that averaged over the human occupied volume. Obvious differences can be found under the two exposure conditions. Compared to the plane-wave exposure, the SAR for the top-loaded monopole exposure exhibited more non-uniform distribution. Similar to the incident electric field distribution, the high SAR area appeared in the upper part of the body.

Changing the distance d from the antenna as a parameter, we compared the whole-body average SAR between the top-load monopole exposure and the plane-wave exposure, which is shown in Fig. 8. In each of the locations the incident electric field intensity for the plane-wave exposure was set to the average level in the human-occupied volume for the top-loaded monopole exposure with 1 W input power. As can be seen from the result in Fig. 8, the maximum whole-body average SAR occurred at $d = 1.2$ m. This may be explained by the fact that the top-loaded monopole antenna had a null directivity towards the floor just below it, and the radiated electric field decreased with the distance d . The two characteristics determined the maximum in Fig. 8. Comparing the whole-body average SAR values between the two exposure conditions, we found that the plane-wave exposure gave a similar SAR estimation, i.e., within $\pm 20\%$ from the actual top-loaded monopole exposure, although strong non-uniformity of the field distributions exists due to the reflection from the concrete walls and the radiation pattern of the antenna. Especially, at the nearer distances with larger SARs, the plane-wave exposure gave an overestimate compared to the top-loaded monopole exposure.

In Table 2 we compared not only the whole-body average SAR but also the one-gram and ten-gram averaged spatial peak SARs between the two different exposure conditions. In the top-loaded monopole situation the distance d between the antenna and the human occupied volume as shown in Fig. 1(b) was 1.2 m, and in the plane-wave ex-

posure situation the incident electric field intensity was set to the field average within the human occupied volume at $d = 1.2$ m in the top-loaded monopole situation. This was named as Case 1. In addition, to evaluate the non-uniformity effect of the incident electric fields, we also shifted the human body by a deviation of 10 cm (Case 2) or 20 cm (Case 3) to the positive x-direction from the center of the cross-section of the underground passage. In Table 2, the second column lists the whole-body average SAR. The third and fourth columns list the one-gram and ten-gram averaged spatial peak SARs in the whole body, and the fifth and sixth columns list the one-gram and ten-gram averaged spa-

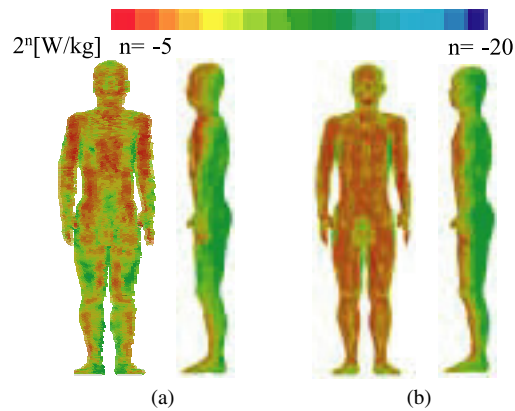


Fig. 7 Surface SAR distributions. (a) top-loaded monopole and (b) plane wave.

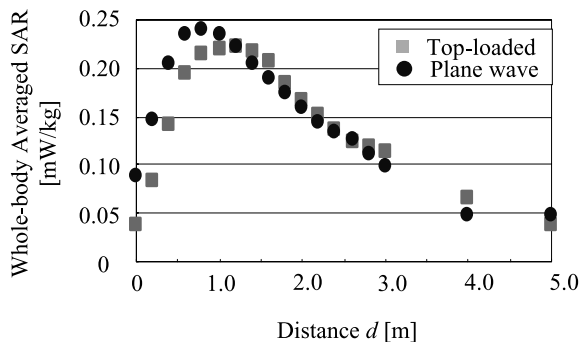


Fig. 8 Whole-body average SAR versus distance d .

tial peak SARs in the head and trunk. As can be seen from Table 2, the whole-body average SAR kept at a similar level but the spatial peak SAR appeared in different locations of the human body and varied to a large extent. Paying attention to the head and trunk region, we found that the ten-gram averaged spatial peak SAR appeared in the chin for the plane-wave exposure but shifted to the stomach, nose or chest for the top-loaded monopole exposure. The plane-wave exposure may result in some lower peak SAR values compared to the top-loaded monopole exposure in some cases. For example, the plane-wave-derived ten-gram averaged spatial peak SAR was only about 1/3 of the top-loaded monopole antenna in Case 2. This result implied the importance of modeling actual underground environment in the peak SAR evaluation for the base station exposure. Based on the above results, as long as the electric field from the base station antennas is not larger than the reference level, the whole-body average SAR is unlikely to exceed the basic safety limit, i.e., 0.08 W/kg.

4. Conclusion

The base station exposure in an underground environment is quite different from a plane-wave exposure. For such a non-uniform exposure, it is unclear whether the whole-body average SAR is under the basic safety limit when the incident electric field averaged over a human-occupied volume meets the reference level. In this study, using a hybrid technique that combines the ray-tracing method for the incident electric field calculation and the FDTD method for the SAR calculation, we investigated the relationship of the SARs between an actual base station antenna exposure in an underground passage and a plane-wave exposure. The results show that the plane-wave exposure overestimated the whole-body average SAR in most cases, although this was not always true for peak SAR. The finding revealed the usefulness of the present uniform-exposure-based reference level for the whole-body average SAR evaluation. It also implied the necessity of modeling actual underground environment for high-precision local peak SAR evaluation.

In future, the plan is to perform a more extensive investigation for various base station exposures in the under-

Table 2 Whole-body average SAR and spatial averaged peak SAR under 1/10 of the reference level of electric fields.

	Whole body average	Whole body 1 g	Whole body 10g	Head and trunk 1 g	Head and trunk 10 g
Top-loaded (Case 1)	0.550 (center)	21.00 (hand)	9.88 (shoulder)	13.25 (nose)	6.93 (stomach)
Top-loaded (Case 2)	0.531 (10cm)	45.71 (nose)	20.18 (nose)	45.71 (nose)	20.18 (nose)
Top-loaded (Case 3)	0.536 (20cm)	16.22 (hand)	8.97 (shoulder)	14.79 (chest)	7.68 (chest)
Plane wave	0.546	37.15 (hand)	15.49 (hand)	15.45 (nose)	6.94 (chin)

Unit:[mW/kg]

Case 1: Human-occupied volume is in the center of the cross-section of the passage.

Case 2: 10 cm shift from the center; Case 3: 20 cm shift from the center.

ground environment, and to attempt to derive a quantitative factor in order to relate the volume-averaged field level for a non-uniform exposure to a plane-wave exposure.

Acknowledgement

The authors would like to thank Dr. S. Watanabe, National Institute of Information and Communications Technology, for providing us with the Japanese whole body human model.

References

- [1] International Commission on Non-Ionizing Radiation Protection, "Guidelines for limiting exposure to time-varying electric, magnetic, and electromagnetic fields (up to 300 GHz)," *Health Physics*, vol.74, no.4, pp.494–522, April 1998.
- [2] IEEE Std C95.3-2002, "IEEE recommended practice for measurements and computations of radio frequency electromagnetic fields with respect to human exposure to such fields, 100 kHz–300 GHz," 2002.
- [3] K.S. Kunz and R.J. Luebbers, *The Finite Difference Time Domain Method for Electromagnetics*, CRC Press, Boca Raton, FL, 1993.
- [4] P. Bernardi, M. Cavagnaro, S. Pisa, and E. Piuze, "Human exposure to radio base-station antennas in urban environment," *IEEE Trans. Microw. Theory Tech.*, vol.48, no.11, pp.1996–2002, Nov. 2000.
- [5] T. Imai, Y. Inukai, and T. Fujii, "Indoor microcell area prediction system using ray-tracing method," *IEICE Trans. Commun. (Japanese Edition)*, vol.J83-B, no.11, pp.1565–1576, Nov. 2000.
- [6] T. Imai, "Prediction of propagation characteristics in tunnels using ray-tracing method," *IEICE Trans. Commun. (Japanese Edition)*, vol.J85-B, no.2, pp.216–226, Feb. 2002.
- [7] H. Jiang and H. Arai, "FDTD analysis of low profile top loaded monopole antenna," *IEICE Trans. Commun.*, vol.E85-B, no.11, pp.2468–2475, Nov. 2002.
- [8] T. Nagaoka, S. Watanabe, K. Sakurai, E. Kunieda, S. Watanabe, M. Taki, and Y. Yamanaka, "Development of realistic high-resolution whole-body voxel models of Japanese adult males and females of average height and weight, and application of models to radio-frequency electromagnetic-field dosimetry," *Phys. Med. Biol.*, vol.49, pp.1–15, 2004.
- [9] C. Gabriel, "Compilation of the dielectric properties of body tissues at RF and microwave frequencies," *Brooks Air Force Technical Report AL/OE-TR-1996-0037*, 1996.



Masayuki Komatsu received his B.E. degree and M.E. degree in electrical and computer engineering from Nagoya Institute of Technology, Nagoya, Japan, in 2004 and 2006, respectively. He is currently with Toyota Industries Corporation.



Osamu Fujiwara received his B.E. degree in electronic engineering from Nagoya Institute of Technology, Nagoya, Japan, in 1971, and his M.E. and D.E. degrees in electrical engineering from Nagoya University, Nagoya, Japan, in 1973 and in 1980, respectively. From 1973 to 1976, he worked in the Central Research Laboratory, Hitachi, Ltd., Kokubunji, Japan, where he was engaged in research and development of system packaging designs for computers. From 1980 to 1984 he was with the Department of Electrical Engineering at Nagoya University. In 1984 he moved to the Nagoya Institute of Technology, where he is presently a professor at the Graduate School of Engineering. His research interests include measurement and control of electromagnetic interference due to discharge, bioelectromagnetics and other related areas of electromagnetic compatibility. Dr. Fujiwara is a member of the IEE of Japan and of the IEEE.



Shinji Uebayashi received the B.E., M.E. and D.E. degrees from Nagoya University, Japan, in 1981, 1983 and 1986, respectively. From 1986 to 1992 he was with NTT Laboratories, Yokosuka, Japan, where he worked on the development of digital cellular system (PDC). Since 1992 he has been with NTT DoCoMo, Inc., where he worked on the development of W-CDMA cellular system and EMC for cellular systems. He is currently the Director of EMC Laboratory in NTT DoCoMo, Inc. His research interests include electromagnetic compatibility and bio-electromagnetics. Dr. Uebayashi is a member of the Institute of Electrical Engineers of Japan (IEE), Japanese Society for Medical Biological Engineering (BME), and of Bioelectromagnetics Society (BEMS).



Jianqing Wang received his B.E. degree in electronic engineering from Beijing Institute of Technology, Beijing, China, in 1984, and his M.E. and D.E. degrees in electrical and communication engineering from Tohoku University, Sendai, Japan, in 1988 and 1991, respectively. He was a Research Associate at Tohoku University and a Research Engineer at Sophia Systems Co., Ltd., prior to joining the Nagoya Institute of Technology, Nagoya, Japan, in 1997, where he is currently a Professor. His research interests

include biomedical communications and electromagnetic compatibility.